3-D Seismic Response of Liquefaction-Susceptible Improved-Soil Deposits

B.A. Bradley
University of Canterbury, New Zealand

SUMMARY:
This paper presents the effect of various configurations of soil improvement on the seismic response of liquefiable soil deposits using 3-dimensional seismic effective stress analysis. Using a case study of the down-hole seismic array site at Port Island, Kobe, Japan; nine different soil improvement geometries are considered by changing both the number, and wall thickness, of improved soil cells for the site. The salient features of the ground response are presented, including: (i) peak surface acceleration, displacement and response spectra; (ii) excess pore pressure, stress path, and stress-strain response of the enclosed unimproved soil; and (iv) peak deformations of the improved soil. The results demonstrate the complexity of seismic response and interaction between improved and enclosed liquefaction-susceptible native soils when subjected to strong ground shaking, as well as the wealth of insightful information that advanced effective stress analyses can provide for assessing the seismic response of such soil deposits.

Keywords: seismic response, liquefaction, jet grouting ground improvement, stress-density model

1. PROBLEM CONSIDERED

Soil liquefaction, which results from a build-up of excess pore water pressures in loose saturated soils, leads to an almost complete loss of strength and stiffness of soil and consequently unacceptably large deformations. Figure 1.1 illustrates the extensive region over which liquefaction occurred at Port Island during the 1995 Kobe earthquake.

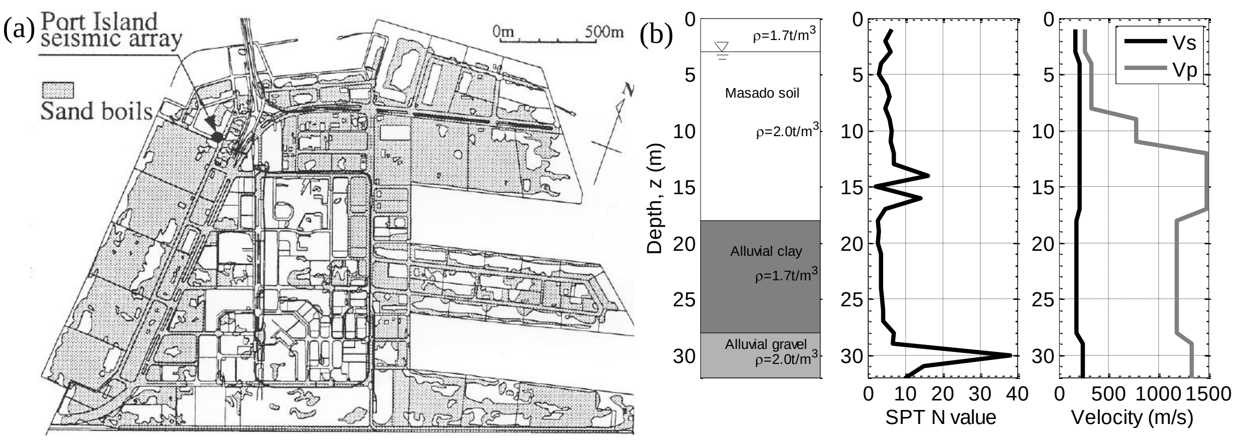

Figure 1.1. (a) Liquefaction observed in the 1995 Kobe earthquake at Port Island; and (b) properties of the downhole array considered.

The effects of soil liquefaction on strong ground motion can be understood by examining the strong ground motions recorded at various depths at the Port Island seismic array (see Figure 1.1) which are shown in Figure 1.2. It can be seen that the incoming ground motion at a depth of 32m has a peak acceleration of 0.6g, and that the intensity and frequency content of the ground motion is preserved in propagating through alluvial gravel and clay soils from 32m depth to 16m depth. On the other hand, the ground motion observed at the surface (GL-0m) is notably different from those observed at depth, with a significant reduction in acceleration amplitude and removal of high frequency ground motion from t=5s onwards.

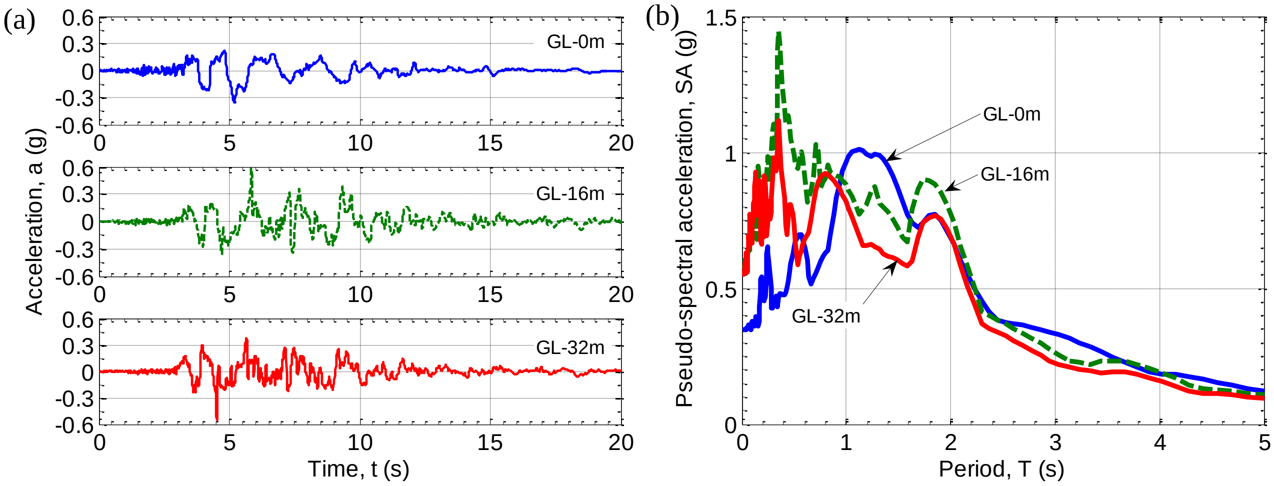

Figure 1.2 Observed ground motion at the Port Island array in the 1995 Kobe earthquake: (a) acceleration time series; and (b) pseudo-acceleration response spectra (5% damping).

In order to illustrate the physical mechanisms which result in the observations in Figure 1.2, as well as the capability to model them, a 1D finite element analysis of a single column of soil was performed. The alluvial gravel and clay were modelled as elastic materials, while the sand layer of Masado soil was modelled using the elastic-plastic Stress-Density (S-D) model of Cubrinovski and Ishihara (1998). The S-D model parameters adopted for Masado soil are given in Cubrinovski et al. (2000). Figure 1.3 compares the predicted acceleration time series at the ground surface and 15m depth with those observed. It can be seen that the computational model is able to capture the key features of the seismic response of the soil deposits.

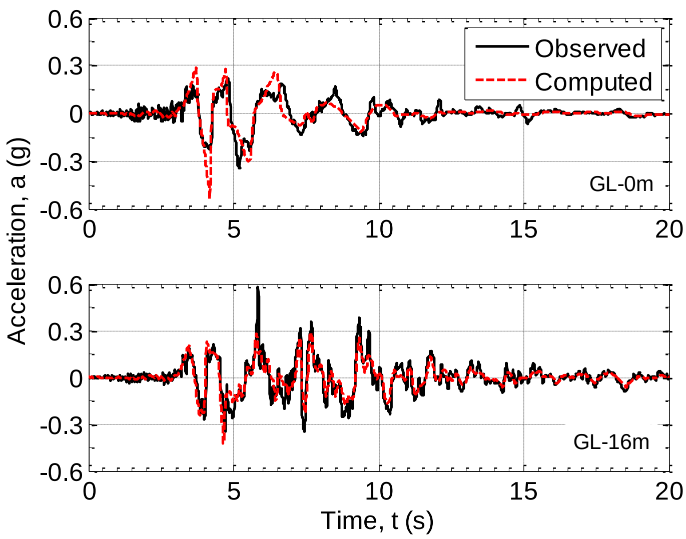

Figure 1.3. Comparison of observed and predicted ground motion at the Port Island array

Figure 1.4 illustrates the seismic response of the Masado soil at a depth of 10.5m. Figure 1.4 illustrates that excess pore pressures rapidly develop after the onset of strong ground motion shaking at approximately 3s, and liquefaction first occurs at approximately 5s (for which the excess pore water pressure ratio, EPWPR, is equal to 1.0). Figure 1.4 also illustrates the stress path, and stress-strain response of the soil, where it can be seen that as the effective stress of the soil decreases the shear stiffness and strength of the soil also rapidly decrease.

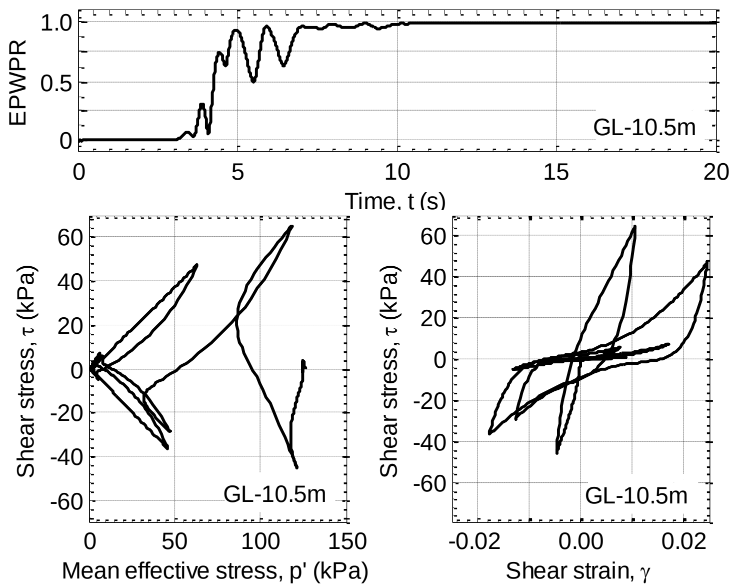

Figure 1.4. Illustration of pore pressure development, stress path, and stress-strain response of soil at depth of GL-10.5m

2. FINITE ELEMENT MODEL WITH GROUND IMPROVEMENT

The seismic performance of soil deposits can be improved using various ground improvement techniques. Jet grouting is one such technique which involves the horizontal injection of cementitious material into the soil under high pressures. A key consideration in the use of jet grouting (and other improvement techniques) is the determination of an appropriate geometry of improved cells or walls. Obviously such a consideration involves a balance between the improved seismic performance, and increased cost associated with a larger volume of grout injection. However, because the improved soil provides kinematic constraint to the surrounding native soil, it is possible that different improved soil geometries with the same total improved area may provide different levels of performance improvement. In an effort to investigate such a question, nine different geometries of soil improvement were considered for a hypothetical site with overall plan dimensions of 24m by 24m. Table 2.1 provides a list of the different improvement geometries considered, while Figure 2.1a provides schematic illustrations of the geometries in plan-view. In summary, three different cell configurations were considered: 1 cell, 4 cell, and 9 cell. For each cell configuration, different wall widths were selected. For each of the 9 cases considered, the improved area ratio, R_{IA}, defined as the ratio of improved to total soil area (in plan). It is noted that R_{IA} for the different wall widths for each cell configuration are essentially equal, implying approximately equal material costs in construction. Because the potentially liquefiable soil layer extends from the ground surface to 18m depth, the top 18m of soil was considered for ground improvement.

Table 2.1. Details of improved soil geometries

Case ID	No. of cells	Wall width, W (m)	Improved area ratio, R_{IA}
1C-2	1	2.0	0.31
1C-3	1	3.0	0.44
1C-4	1	4.0	0.56
4C-1.5	4	1.5	0.34
4C-2	4	2.0	0.44
4C-2.5	4	2.5	0.53
9C-1	9	1.0	0.31
9C-1.5	9	1.5	0.44
9C-2	9	2.0	0.56

(a)

(b)

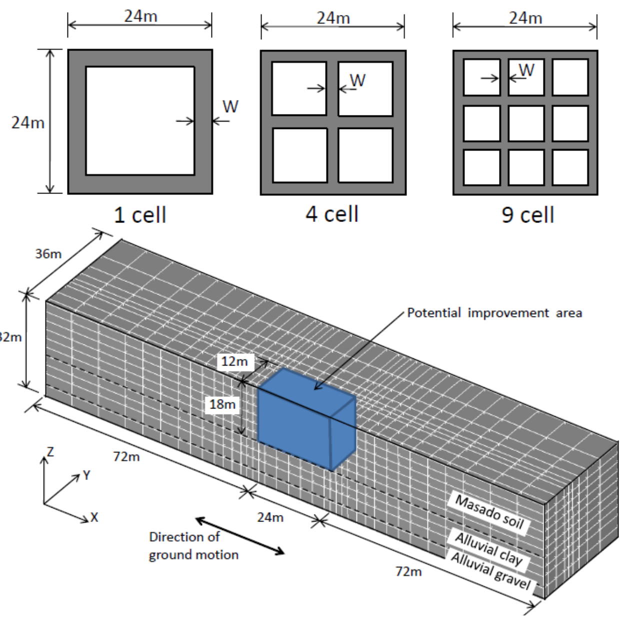

Figure 2.1. (a) Considered improved soil geometries; and (b) schematic illustration of the finite element model used indicating the area considered for ground motion improvement (note that X-symmetry was employed)

Figure 2.1b illustrates the finite element mesh which was used for performing the various analysis cases considered. The same vertical stratigraphy as that for the Port Island seismic array was considered. The 3-D effective stress modelling of the Masado soil layer was based on a simplified approach in which pore-pressures were assumed to occur only due to deformation in the principal plane of response (i.e. the x-z plane), and that the response is governed by three-independent shear mechanisms (Cubrinovski et al., 2003). The improved soil was modelled as a linear elastic material with shear stiffness of E=420MPa.

3. RESULTS OF 3-D EFFECTIVE STRESS ANALYSES

As previously noted, a total of 9 different soil improvement geometries were considered. Below, two cases are considered for each number of cells examined in order to demonstrate the salient effects of how the improved soil region affects the dynamic response of the soil deposit. Finally, the results are summarized by comparing all cases based on the improved area ratio. For brevity, discussion of the 9-cell case is omitted, but can be found in Bradley et al. (2012).

3.1. Response of soil inside improved region

In order to illustrate the effects of ground improvement on seismic response consider firstly the response of the soil deposit enclosed within the improved area. Figure 3.1 compares the acceleration and displacement time series of the ground surface at the centre of the soil enclosed within the improved soil region. It can be seen that for the first cycle of strong ground motion, the response is similar for the unimproved and two improved cases, however subsequently the aforementioned degradation in stiffness and strength of the soil in the unimproved case leads to reduced acceleration amplitudes, longer vibration period, and larger peak displacements. On the other hand, the ground improved cases do not show such characteristics. The response for the two considered soil improvement cases is similar, but it is noted that the peak displacement, which occurs at approximately t=5s, is slightly lower for the 1C-4 case as compared to the 1C-2 case.

Figure 3.2 illustrates the acceleration response spectra of the ground motion presented in Figure 3.1. As previously noted it can be seen that in the unimproved case the spectral amplitudes are notably less than the ground improvement cases for T<3 seconds. Interestingly, the reduction in the peak ground acceleration is small, as this occurs early in the response time series, while the peak acceleration response for 1 second period, which requires several cycles of strong ground motion to achieve resonance, is significantly larger in the improved cases.

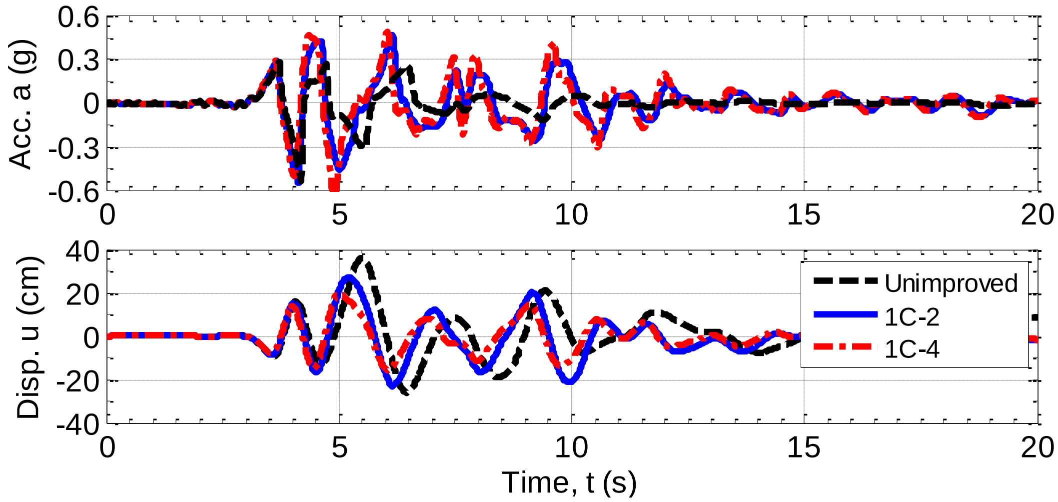

Figure 3.1. Acceleration and displacement at the ground surface for two wall widths in the 1 cell case

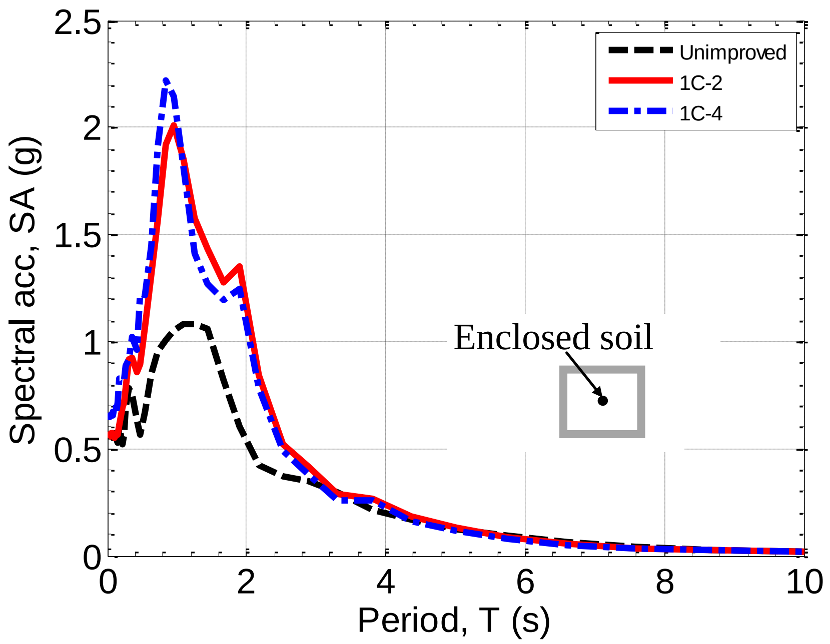

Figure 3.2. Acceleration response spectra of the surface ground motion for two wall widths in the 1 cell case. (5% critical damping)

Figure 3.3 illustrates the response of soil at a depth of 10.5m for the two different soil improvement geometries in comparison to the unimproved case. It can be seen that for the 1C-2 case, liquefaction occurs at essentially the same time as in the unimproved case, however the consequent cyclic shear strains induced are significantly less. In comparison, in the 1C-4 case the occurrence of liquefaction is delayed by several seconds as pore pressures build up at a slower rate. It can be seen that, while complete liquefaction eventually develops in the 1C-4 case, the induced cyclic strains are notably smaller than in the 1C-2 and unimproved cases.

Figure 3.4 illustrates the distribution with depth of peak accelerations, displacements and shear strains at the centre of the soil enclosed in the improved cell. Firstly, it can be seen that shear strains are largest in the Masado soil layer (i.e. depths<18m), with peak shear strains below 0.5% in the underlying alluvial gravel and clay layers. It can also be seen that peak shear strains of nearly 3% occur in the unimproved case compared with 2% in the 1C-2 soil improvement case and 1% in the 1C-4 case. At the ground surface the previously discussed shear strains translate to peak displacements of

36cm, 27cm, and 19cm, for the unimproved, 1C-2, and 1C-4 cases, respectively. It is also pertinent to note that, in terms of peak accelerations, the soil improvement cases generally lead to an increase in peak accelerations in the Masado soil layer, and a reduction in the alluvial gravel and clay layers as a result of less “trapping” of waves in the surface layer.

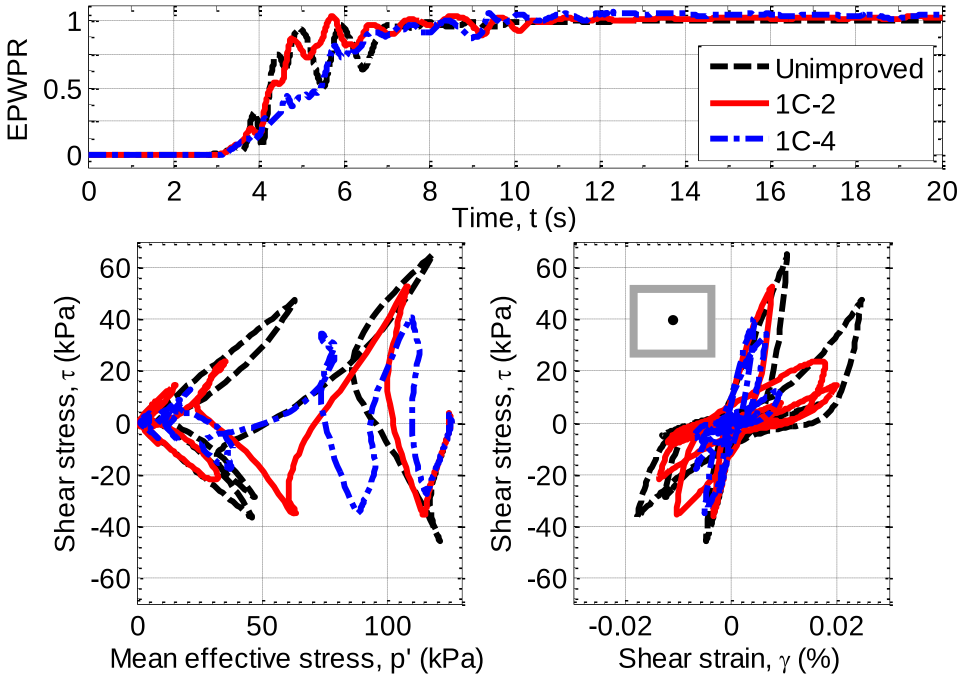

Figure 3.3. Pore pressure development, stress path, and stress-strain response of soil at depth of GL-10.5m for two wall widths in the 1 cell case

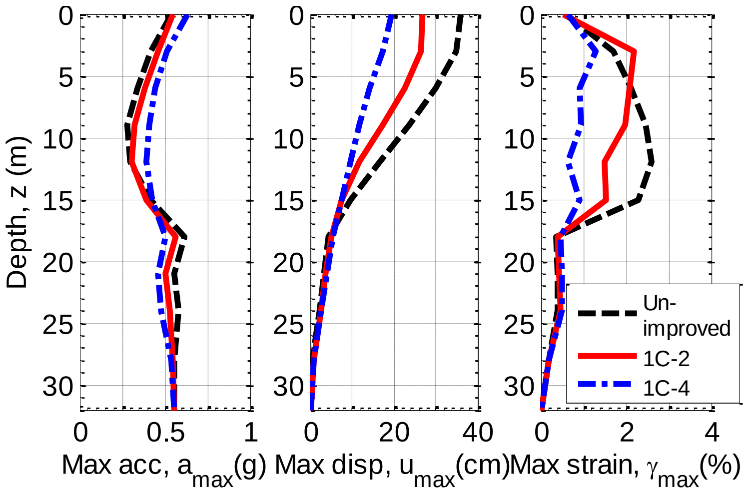

Figure 3.4. Maximum acceleration, displacement, and shear strain with depth at the centre of the 1 cell improved region

3.2. Response of improved soil cell

Figure 3.5 illustrates the displacement with depth of the centre and edge of the improved soil cell, as well as its displacement in plan along the perpendicular face. It can be firstly seen that in the 1C-2 case (i.e. cell width of 2m and length 24m) the differential displacement of the cell wall in plan is significant with the centre of the cell undergoing almost the same displacement as the free-field soil, while the displacement at the cell edges is on the order of half that of the free-field. In the 1C-4 case (i.e. twice the wall width of the 1C-2 case) it can be seen that the differential displacement in plan is less pronounced with peak displacements of approximately 18cm and 16cm at the centre and edge of the cell, respectively. It can also be seen that in the 1C-4 case, and at the cell edge in the 1C-2 case, the displacement with depth is approximately linear, implying approximately constant strain with depth in the improved soil. Finally it is noted that due to the stiffness of the improved soil, the peak displacements at the base of the improved soil edge are greater than that of the surrounding soil, as previously observed by others in the case of deep-soil-mixing (DSM) ground improvement walls (Cubrinovski et al., 2003).

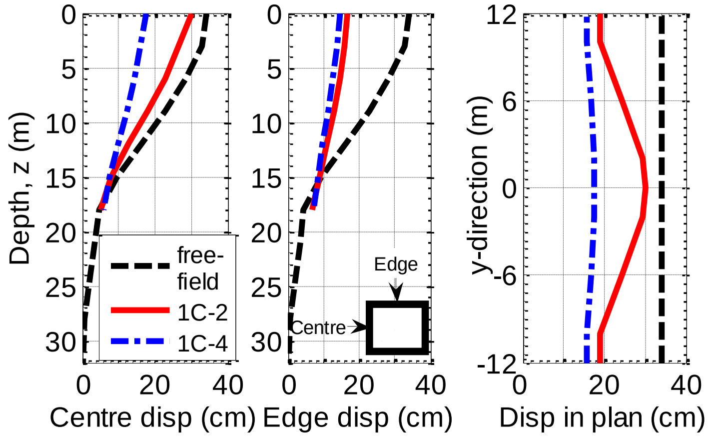

Figure 3.5. Displacements of improved soil centre and edge with depth and displacement in plan (1 cell case)

3.3. Features of the response in the 4 cell case

There are several similarities between the responses of the improved ground in the 4 cell cases and those of the 1 cell cases, and hence discussion here is only given to the notable differences between these.

The surface acceleration and displacement response at the centre of the improved zone in the 4 cell cases was essentially identical to that observed in the 1 cell case (i.e. Figure 3.1). Figure 3.6 illustrates the soil response within the improved soil cell at a depth of 10.5m. Unlike the 1C-2 case shown in Figure 3.3, it can be seen that even for the thin cell wall (i.e. 1.5m) the response in the 4C-1.5 case illustrates that the generation of excess pore pressures occurs at a reduced rate compared with that in the unimproved case. In the 4C-2.5 case, in particular, it can be seen that complete liquefaction (i.e. *EPWPR*=1.0) does not occur at a depth of 10.5m, and hence significantly lower peak shear strains occur.

Figure 3.7. illustrates the peak acceleration, displacement and shear strains with depth at the centre of the 4 cell improved region. Similar, to the results observed in the 1 cell case, it can be seen that soil improvement leads to an increase in peak accelerations in the Masado soil layer, and reduced accelerations in the underlying alluvial gravel and clay layers. It can be seen that displacement and shear strains in the improved cases are similar, and significantly less than the unimproved case. In particular peak surface displacements in both the 4C-1.5 and 4C-2.5 cases are less than 20cm compared with 36cm in the unimproved case. In the 4C-2.5 case, for which as previously noted complete liquefaction does not occur, it can be seen that the peak shear strains are approximately 0.5% which is similar to those in the underlying gravel and clay layers. For the 4C-1.5 case it can be seen that the occurrence of increased pore pressures, particularly at the base of the Masado soil layer, leads to larger shear strains.

Figure 3.8 illustrates the peak displacement with depth at the middle of the perpendicular improved soil cell wall as well as the peak displacements in plan at the ground surface. It can be seen that in the 4C-1.5 case there is some difference in peak displacements in plan, although not as significant as was observed in the 1C-2 case (Figure 3.5). In contrast, the variation in the displacements in plan for the 4C-2.5 case is very small. The displacements with depth at the centre of the wall are similar to those observed in the 1 cell case.

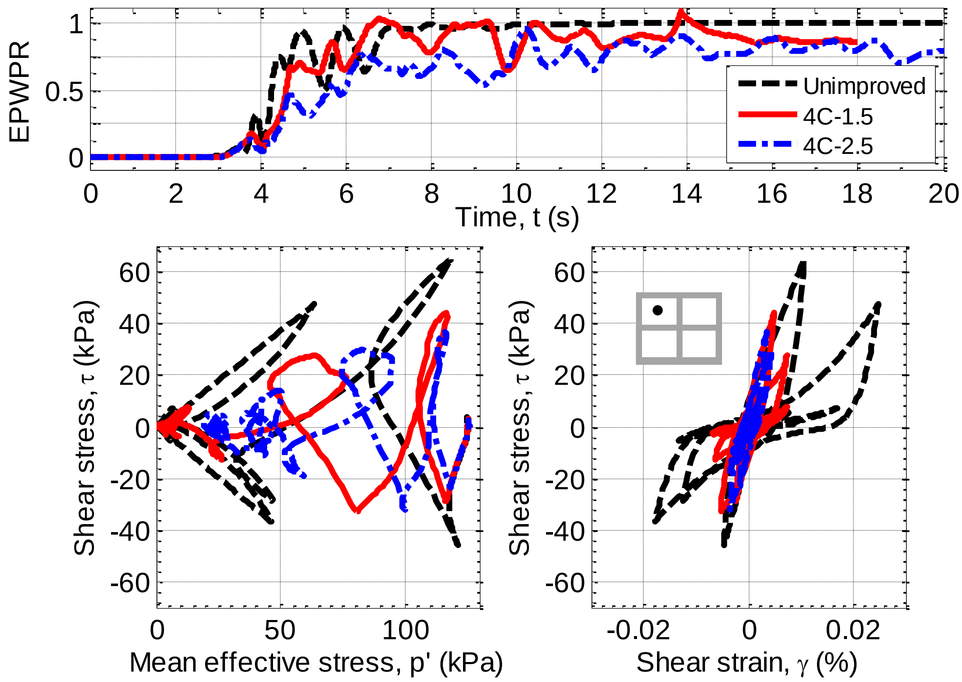

Figure 3.6. Pore pressure development, stress path, and stress-strain response of soil at depth of GL-10.5m for two wall widths in the 4 cell case

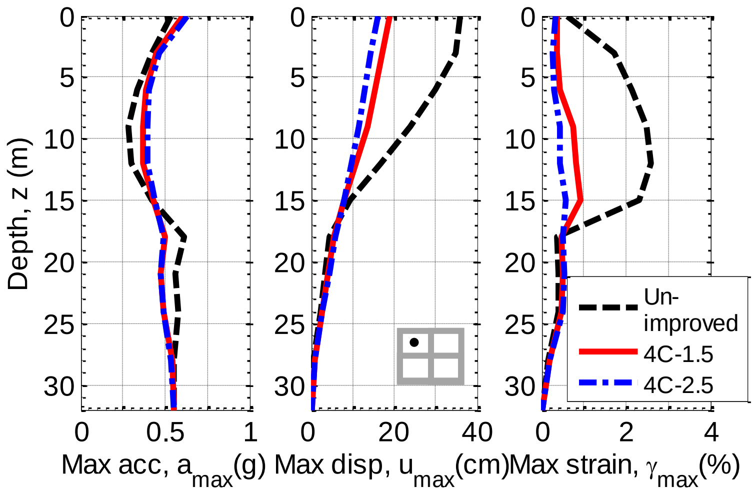

Figure 3.7. Maximum acceleration, displacement and shear strain with depth at the centre of the 4 cell improved region

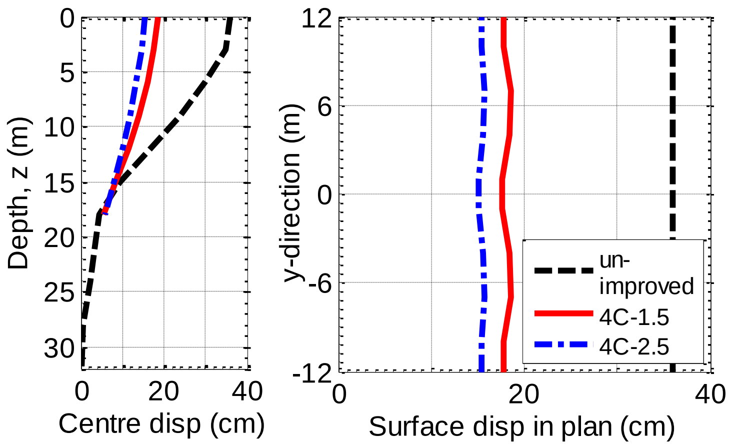

Figure 3.8. Displacements of improved soil centre-line with depth and displacement in plan (4 cell case)

3.4. Summary of effect of soil improvement geometries in terms of improved area ratio, R_{IA}

Figure 3.9a illustrates the peak displacement at the ground surface of native soil at the centre of the soil improvement enclosed region as a function of R_{IA}. Firstly, it can be seen that all 9 improvement geometries are effective at restraining the native soil with peak displacements of the soil enclosed within the ground improvement cells in the range 15-27cm, as compared to the 36cm displacement in the unimproved case. For a given number of cells it can be seen that there is a reduction in peak displacement with increasing R_{IA}, as expected. Finally, it can be seen that for a given R_{IA} value, the 9 cell configuration results in the lowest displacements, followed by the 4 cell case. Figure 3.9b illustrates the pore pressure ratio at the end of ground shaking ($t = 20$s) of the enclosed native soil at a depth of GL-10.5m. It can be seen that complete liquefaction occurs at this depth in the 1 cell case, irrespective of the width of the improved soil. On the other hand, in the 4 cell case it can be seen complete liquefaction does not quite develop, however there is also little dependence of EPWPR on improved wall thickness. Finally for the 9 cell case it can be seen that there is a notable impact of the improved wall thickness, with EPWPR decreasing with increasing improved wall thickness.

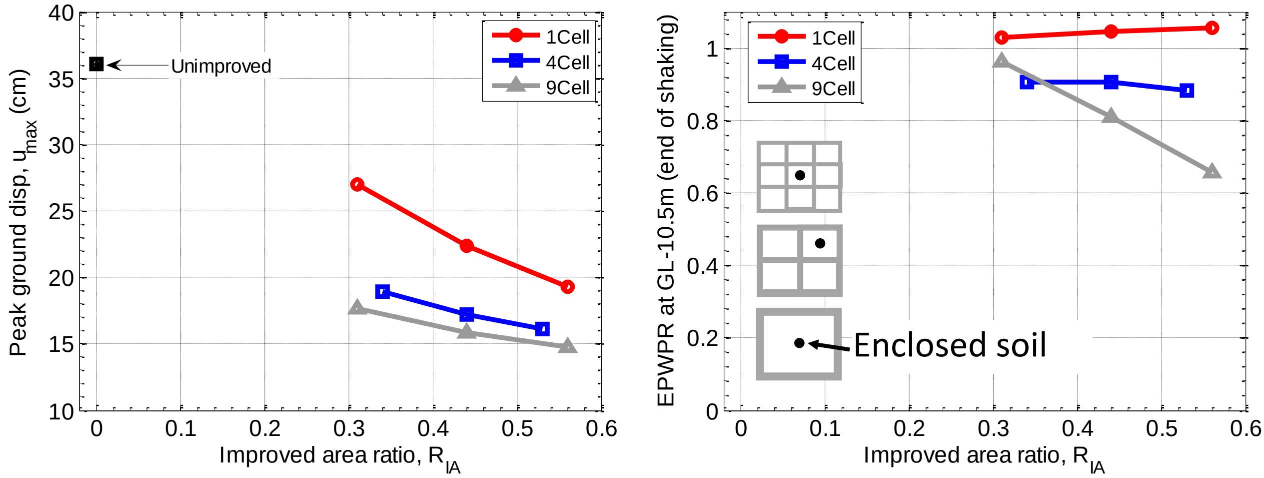

Figure 3.9. (a) peak surface ground displacement; and (b) excess pore water pressure ratio (EPWPR) at the end of shaking (t=20s) at a depth of GL-10.5m of native soil enclosed within the improved area.

It was previously noted, in relation to Figure 3.2, that the use of soil improvement results in an increase in spectral accelerations for short to moderate vibration periods of the ground motion recorded at the surface. This increase in spectral accelerations is important as it means that increased inertial seismic demands may result for structures which are founded on improved soils (although kinematic seismic demands due to foundation deformation will inevitably reduce). Figure 3.10 illustrates the variation in spectral accelerations as a function of R_{IA}. As previously noted, it can be seen that there is little difference between the peak ground acceleration in the improved and unimproved cases, but that the SA(0.5) and SA(1.0) amplitudes are much larger with ground improvement. In the majority of cases it can be seen that increasing the improved area (i.e. increasing the wall width) leads to an increase in spectral amplitudes, although the effect appears to be small (with the exception of the 1 cell case for PGA and SA(0.5)). Interestingly, it can be seen that while the magnitudes of PGA and SA(0.5) are similar for the three different cell configurations, the magnitude of SA(1.0) is larger for the 1 cell configuration followed by the 4 cell and then 9 cell configurations (an overall variation of approximately 10% in SA(1.0)). Examination of the response spectra of the seismic response in the unimproved case in Figure 1.2 illustrated that significant amplification was observed around a vibration period of $T = 1.0 - 1.4$s due to the reduced stiffness of the liquefiable deposit. Hence, while the seismic response and interaction between improved and native soil is clearly complex, it is inferred that the larger SA(1.0) amplitudes observed in Figure 3.10 are the result of the greater stiffness reduction which occurs in the enclosed native soil in the 1 cell case (the reasons for which have been discussed in previous paragraphs), relative to the 4 cell and 9 cell cases.

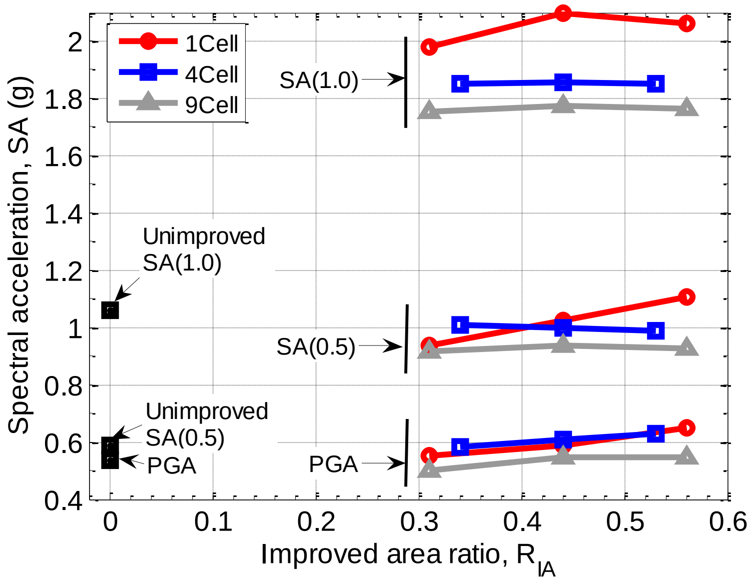

Figure 3.10. Variation in peak spectral acceleration at the surface inside the improved area as a function of the number of cells and the improved area ratio, R_{IA}.

4. CONCLUSIONS

The effects of various soil improvement geometries on mitigating liquefaction in susceptible soil deposits using 3-D seismic effective stress analysis with an advanced constitutive model for sandy soils has been investigated. The salient features of the surface ground motion, peak shear strains, displacements, pore pressures and stress-stain response of the enclosed native soils and improved soil were discussed for each of the considered improvement geometries. It was observed that all of the improved soil geometries were effective at mitigating liquefaction and some of its consequences with reductions in peak surface of the enclosed soil. The 4 cell and 9 cell improvement geometries were the most effective, because in the 1 cell improvement geometry the lateral extent of the enclosed native soil was such that substantial relative displacements occurred, resulting in an inability of the improved soil to prevent significant shear strains and pore pressures, and consequently resulting in large lateral displacements relative to the 4 and 9 cell improvement geometries. Finally, it was also observed that the soil improvement resulted in increased amplitude of the surface ground motion at moderate-to-long periods, but less of an increase at short periods. Hence, liquefaction mitigation via ground improvement will generally result in higher inertial loading for the overlying superstructure.

5. ACKNOWLEDGMENTS

Funding of the first author from the Japan Society for the Promotion of Science (JSPS) is greatly appreciated. Fruitful discussions with Prof. K. Ishihara are greatly appreciated.

6. REFERENCES

Bradley, B.A., Araki, K., Ishii, T. and Saito, S. 2012. Effect of ground improvement geometry on seismic response of liquefiable soil deposits via 3-D seismic effective stress analysis. *Soil Dynamics and Earthquake Engineering (in review)*.

Cubrinovski, M. and Ishihara, K. 1998. State concept and modified elastoplasticity for sand modelling. *Soils and foundations*, **38: 4,** 213-225.

Cubrinovski, M., Ishihara, K. and Furukawazono, K. (2000). Analysis of two case histories on liquefaction of reclaimed deposits. *In: 12th World Conference on Earthquake Engineering* Auckland, New Zealand.

Cubrinovski, M., Ishihara, K. and Shibayama, T. (2003). Seismic 3-D effective stress analysis: constitutive modelling and application. *In:* AL., D. B. E., ed. *Deformation Characteristics of Geomaterials*, Lyon, France. 8.